REPORT DOCUMENTATION PAGE

Form Approved OMB No. 0704-0188

1. REPORT DATE *(DD-MM-YYYY)*	2. REPORT TYPE	3. DATES COVERED *(From – To)*
22-10-2009	Final Report	29 September 2006 - 28-Jan-10

4. TITLE AND SUBTITLE

In-situ measurements of the displacement field around the nose of a projectile during concrete and sand penetration using the Digital Speckle Radiography (DSR) technique.

5a. CONTRACT NUMBER
FA8655-06-1-3057

5b. GRANT NUMBER

5c. PROGRAM ELEMENT NUMBER

6. AUTHOR(S)

Dr. William G Proud

5d. PROJECT NUMBER

5d. TASK NUMBER

5e. WORK UNIT NUMBER

7. PERFORMING ORGANIZATION NAME(S) AND ADDRESS(ES)

University of Cambridge
Cavendish Laboratory
Cambridge CB3 0HE
United Kingdom

8. PERFORMING ORGANIZATION REPORT NUMBER

N/A

9. SPONSORING/MONITORING AGENCY NAME(S) AND ADDRESS(ES)

EOARD
Unit 4515 BOX 14
APO AE 09421

10. SPONSOR/MONITOR'S ACRONYM(S)

11. SPONSOR/MONITOR'S REPORT NUMBER(S)
Grant 06-3057

12. DISTRIBUTION/AVAILABILITY STATEMENT

Approved for public release; distribution is unlimited. (approval given by local Public Affairs Office)

13. SUPPLEMENTARY NOTES

14. ABSTRACT

The experiments proposed in this research project will use a combination of impact testing and advanced image analysis. Targets will be made of MK4 Grout, in order to reproduce the response of geological materials. These will be impacted by projectiles which examine a number of nose geometries e.g. hemi-spherical, conic, ogive. The use of flash X-rays in this system, to capture images during the impact, means that the samples will have to be of a diameter which is small enough to allow good resolution but sufficiently large to avoid edge effects. The targets will be supported by Kevlar, or similar, fabric in order to maintain target integrity until late in the impact process. This will allow the deformation fields around a projectile tip and also in the bulk of the material to be examined. The analysis element is based on Speckle Cross Correlation and is described in some detail below.

15. SUBJECT TERMS

EOARD, Displacement Field, Penetrator

16. SECURITY CLASSIFICATION OF:			17. LIMITATION OF ABSTRACT	18, NUMBER OF PAGES	19a. NAME OF RESPONSIBLE PERSON
a. REPORT	b. ABSTRACT	c. THIS PAGE			WYNN SANDERS, Maj, USAF
UNCLAS	UNCLAS	UNCLAS	UL	38	19b. TELEPHONE NUMBER *(Include area code)* +44 (0)1895 616 007

EOARD Final Report – Digital Speckle Radiography in the Penetration of Granular Materials

Grant Number - 063057

John Addiss, Adam Collins, William Proud

Fracture and Shock Physics Group,
Cavendish Laboratory,
J J Thomson Avenue,
Cambridge, CB3 0HE,
United Kingdom.
Tel 01223 337205
e-mail wgp1000@cam.ac.uk

April 2009

1. Overview

The research presented in this report outlines a series of experiments using digital speckle radiography (DSR) to investigate the penetration of granular materials by long rod impactors. This research is funded by EOARD, London, Elgin Air Force Base, Florida and DTRA under grant number 063057. This report continues on from previous progress reports (PCS reports SP1182 and SP1191) where the technique of DSR is explained in more detail.

The experiments involve impacting a cylindrically confined sample of sand (100 mm diameter, 150 mm length) with mild steel rod projectiles (length 100 mm, diameter 10 mm). By carrying out a number of experiments with increasing time delays a sequence of images showing the temporal progression of the penetration can be generated. Experiments were carried out using flat ended projectiles and projectiles with ogive 2 nose cones. Detailed displacement maps showing the local response of the material to penetration were generated for both projectile types.

The experiments show that the response of the material is to flow away from the projectile. A cone shaped area of material is set moving longitudinally (parallel to the rod axis). This area extends ahead of the nose of the projectile and maintains a constant angle relative to the rod axis throughout the sequence of images. The extent to which material ahead of the projectile tip is disturbed increases during the early stages of the impact (up to 350 μs, or a depth of around 4 cm), but then appears to remain relatively constant for the remainder of the penetration. This suggests some form of steady-state motion is being reached, something that is confirmed by the velocity profiles for the rods which show an early significant drop in velocity followed by a plateau of relatively constant penetration velocity.

Comparing the behaviour of the ogive and flat ended rods it can be seen that for a given time since impact the ogive rod achieves a greater penetration depth. The displacement fields show that the overall pattern of displacements occurring is the same for both rod types, but that more significant deformation of the material ahead of the rod tip is observed for the flat ended rods. The velocity profiles show that the rods with ogive tips plateau at a higher velocity than those with flat ends. This suggests that the ogive rods are depositing less energy within the material, this agrees well with the observation that less material ahead of the rod is set moving.

2. Experimental Work

2.1 Sand

The sand used in all of the following experiments is a fine concrete sand provided by Cardigan Sand & Gravel Co Ltd (Penparc, Cardigan, Ceredigion, SA43 1RB). The particle size distribution (provided by the manufacturer) is given in figure 1. The sand ranges in size from fractions of a mm up to a few mm.

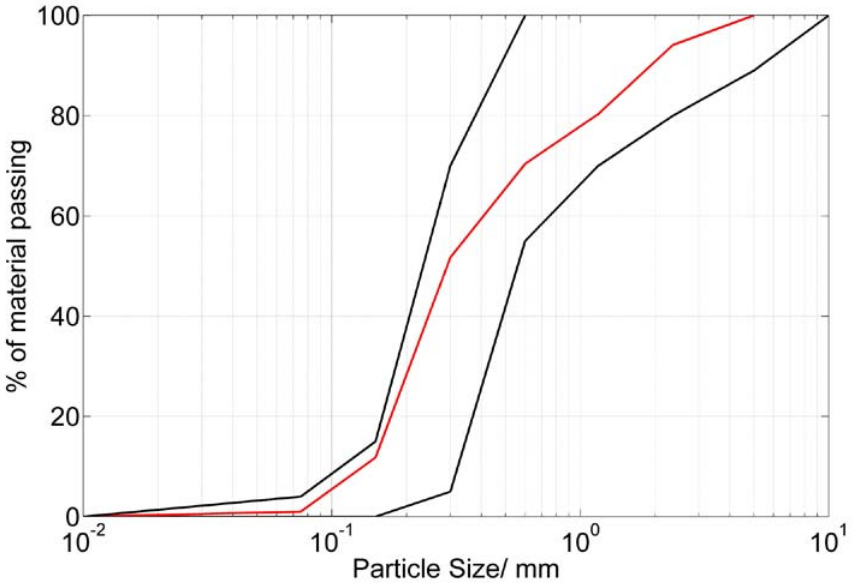

Figure 1. Particle size data for the sand showing the minimum, average and maximum fraction passed against sieve size (manufacturers data)

In order to maintain a uniform water content throughout all of the experiments the sand was baked in an oven at a temperature of 80^0C for a period of 24 - 36 hours before each experiment. This meant that the sand was left with very little water content. Previous experiments have shown that the water content can have a significant effect on the response of the sand to impact. Wet sand appears to dissipate energy more rapidly causing the deformation to drop off more rapidly ahead of the projectile. Using dry sand firstly eliminates the variation that would be caused by a variable water content. Secondly, larger and more measurable displacements are likely to be produced and the deformation process in front of the rod will therefore be more easily visible.

2.2 Flash X-ray System

A flash X-ray system produces a very intense, short duration burst of X-rays (< 100 ns in duration). Such a system is ideally suited for studying high-speed events, such as objects moving at high velocity. The pulse of X-rays is produced by accelerating an intense pulse of electrons, with a small spatial spread, into an X-ray source, usually a tungsten cathode.

A Scandiflash TA400 flash X-ray system was used for these experiments. It produces a pulse of X-rays with a duration of approximately 70 ns and energy ranging from 55-150 keV. The system has a very well characterised X-ray output energy versus charging voltage.

Images are captured using an X-ray cassette (AGFA Curix Ortho Regular cassette). These contain two medical intensifier screens consisting of a polyester base coated in a layer of rare earth phosphors. The image is recorded on X-ray film (AGFA Curix HT1.0006 Plus Medical X-ray Film). The film is subsequently developed by hand using Kodak developing products (Kodak RP X-OMAT LO Developer/replenisher and Fixer/replenisher).

2.3 Preliminary Experiments

A series of preliminary experiments was carried out in order to determine the optimal sample size and lead particle size combination. A number of conflicting requirements must be considered. The sample size should to be large relative to the size of the grains of sand so that there is enough material to be representative of the properties of the bulk material. The sample also needs to be large relative to the diameter of the penetrator, such that compaction waves do not reach the boundaries of the sample until as late as possible.

As the sample size is increased, the contrast on the X-ray images is reduced (for a given size of lead particle the relative increase in X-ray absorption achieved by including the particle gets less as the thickness of sand increases). If the sample is too large there will be insufficient contrast on the images to carry out DICC. The errors in DICC are also increased for blurry images with reduced contrast. To improve the contrast in large samples it is necessary to use relatively large lead particles (around 1 mm in size) so that they absorb a greater fraction of the X-ray intensity, and show up more clearly. This in turn causes problems as the minimum sub-image size required to encompass at least three speckles increases with the speckle size. If the sub-image size

becomes too large the resolution of the displacement map is severely compromised.

In order to choose a sample size and lead particle size combination which is an appropriate compromise of these requirements, a wedge of sand was constructed and a series of different types of lead particles were applied to the bottom surface. The wedge had a maximum depth of 15 cm of sand. The lead ranged in diameter from 150 μm to around 1 mm, the details are given in table 1.

Lead type	Manufacturer	Size
Shot	Sigma-Aldrich	1 mm
30 mesh	Aldrich	< 0.60 mm
100 mesh	Aldrich	< 0.25 mm
Granulated	Sigma-Aldrich	0.2 mm
Lead Powder	Goodfellow	150 microns

Table 1. Types of lead included on the sand wedge

An X-ray image of this wedge allowed comparison of the most suitable type of lead particle for a given thickness of sand. For thicknesses over 8~cm, only the lead shot was clearly visible and other lead sizes did not give sufficient contrast for DICC to be successful. The most suitable lead type for these experiments was therefore the lead shot.

The manufacturers details give the average diameter of this lead as 1 mm. To verify this, a series of photographs of the lead were taken using an optical microscope. The images were analysed using the freely available ImageJ software, to determine the particle size distribution from over 500 particles. The results are shown in figure 2. Ideally, the lead particle size should be closely matched to the size of the particles of sand, to ensure that the lead particles behave as part of the bulk material. In this case, the lead particles are slightly larger than the mean sand particle size, but not significantly so - the mean lead particle size is 1 mm, the mean sand particle size is around 0.5 mm.

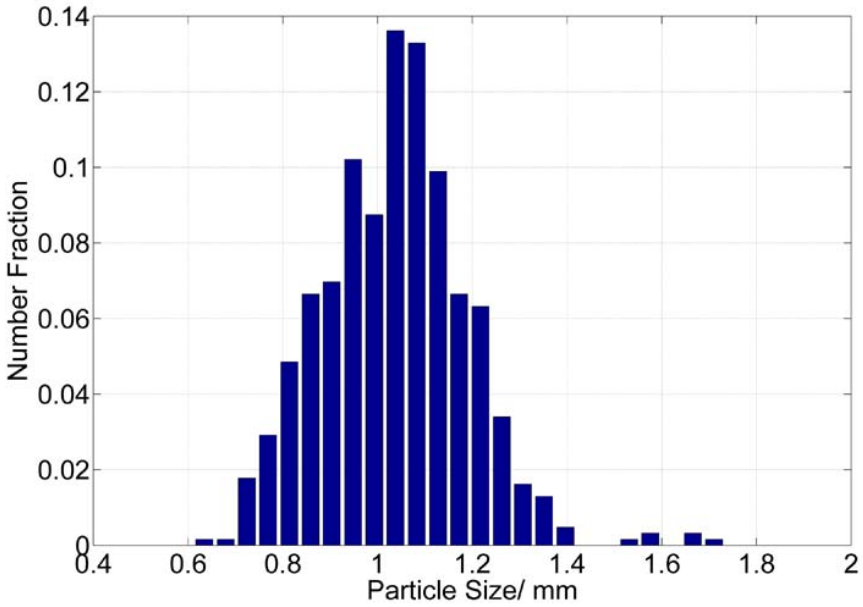

Figure 2. Particle size data for the lead shot, the mean particle size is around 1 mm, a little larger than the mean particle size of the sand.

Having identified suitable types of lead for larger samples, a second sand wedge (with a maximum depth of 20 cm) was constructed. Lead shot was randomly scattered over the surface at a coverage of around 30%. An X-ray image of this wedge is shown in figure 3. This image shows that the contrast is sufficient for DSR for thicknesses of sand up to, and possibly even beyond, 20 cm (the lead shot is clearly visible and the image is not significantly blurred). The maximum thickness that can be used in the experiments will be less than this, due to the strong X-ray absorption of the experimental setup (a sturdy plastic container and a thick plastic lid on the catch chamber will both absorb X-rays). A sample size around 10 cm at the thickest point proved optimal for the experimental setup. This gives good contrast in the images, and is sufficiently large relative to the diameter of the penetrators to allow for a significant depth of penetration before compaction fronts significantly interact with the confinement.

In order to use the DICC technique to investigate the flow of the material, it is essential that the presence of the lead shot does not interfere excessively with the flow, or alter the material response. In order to investigate, this some preliminary experiments were carried out to measure the force experienced by a projectile being slowly pushed into a box of sand, with and without a layer of scattered lead. A box with internal dimensions of 80 mm by 85 mm by 90 mm was used. The box had two removable plastic sides and was designed such that is was possible to seed a layer of lead across a plane in the centre.

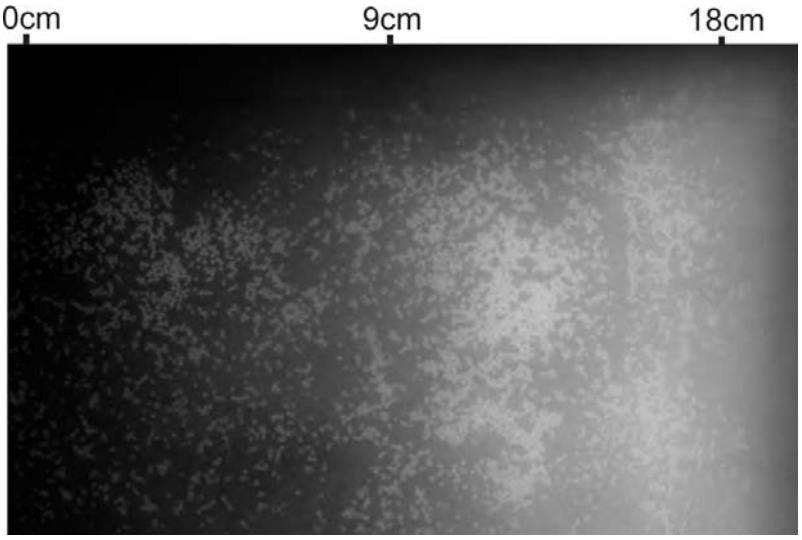

Figure 3. An X-ray of a wedge of sand with a maximum depth of 20 cm seeded with lead shot

An Instron workstation, capable of controllably penetrating the sample at a lower rate (4 mm/min), was used to push a flat ended projectile into the centre of the box. The Instron machine records the vertical force experienced by the rod for a given depth of penetration. This experiment was performed a number of times on loosely packed sand, with and without a seeded layer of lead shot present covering 30% of a vertical plane. The results are shown in the graph in figure 4.

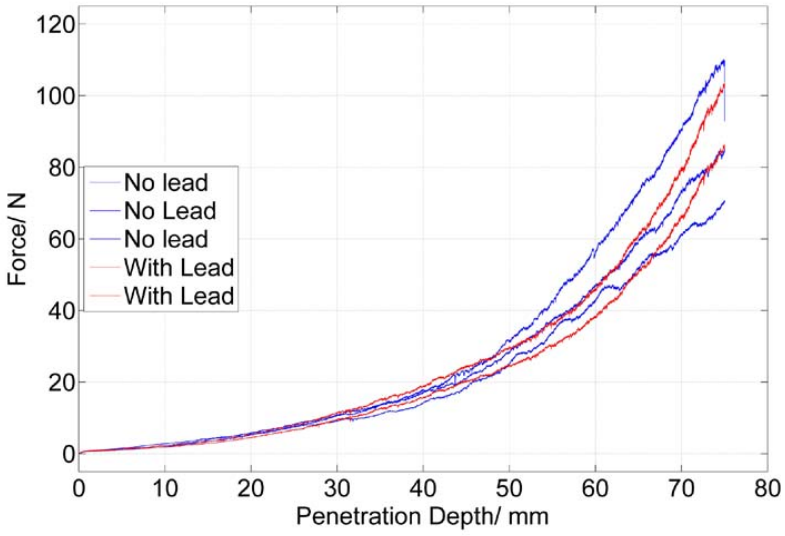

Figure 4. Vertical force versus penetration depth for experiments on samples with and without a seeded layer of lead.

Figure 4 demonstrates that adding a layer of lead to the material had no significant effect on the vertical force experienced by the rod (any difference is

less than the natural variation between samples), and that adding a layer of lead has not altered the response of the material. It is concluded that a coverage of up to 30% of lead can be used without interfering with the behaviour of the sand.

2.4 Sample Design

Producing a cylindrically confined and symmetric sample, containing an internal plane of scattered lead, poses a number of experimental challenges. Initial attempts involved the use of an extruded acrylic tube of internal diameter 100 mm. The tube was cut in half to allow the two sides to be independently filled with sand, and to allow a scattering of lead shot to be applied to the surface of one half. The two halves were then recombined to form a cylinder. This approach was unsuccessful due to the release of hoop stresses (generated in the cylinder during formation) when the cylinder was cut in two. The release of these stresses deformed the two halves of the cylinder, such that the two sections no longer fitted together to make a perfect cylinder. Instead, a gap was formed lengthwise along the cylinder along the join. This gap meant that the sample was not suitably confined and that there was no longer cylindrical symmetry.

The most accurate method of producing a uniform, symmetrical cylinder which could be separated into sections was to bore a cylindrical hole out of a solid block of polycarbonate. The resulting sample holder is shown in figure 5. It has a length of 150 mm and the central bore has a diameter of 100 mm. The cylinder is split lengthwise into two sections. It is cut so that one of the sections is bigger than the other (80 mm high compared to 60 mm). The purpose of this offset is to allow a layer of lead to be scattered over the central plane in the larger section, and to then be covered by a 10 mm layer of sand before the cylinder is reassembled. This minimises any disruption to the layer of lead when the cylinder is reassembled.

When the two sections have been prepared a sheet of Mylar is used to provide a seal for the smaller section so that sand is unable to escape when it is turned upside down and brought back into contact with the larger section. The two sections are lightly bolted on one side and the sheet of Mylar is then slowly removed from the sample. The advantage of having the two sections cut off-centre is that the Mylar is not resting directly on the layer of lead, if this was the case the lead shot would likely be disturbed and dragged to one side when the Mylar was removed, therefore ruining the speckle pattern. Instead, because the layer of lead is covered by a centimetre of sand, it is disturbed little by the removal of the Mylar. The sample holder is tightly bolted

together using five bolts along each side to produce a tightly confined and symmetrical sample. The cylinder of sand is contained at each end by a thin piece of corrugated card, this has relatively little strength while providing sufficient support for the weight of sand. The sample holder is shown in figure 5.

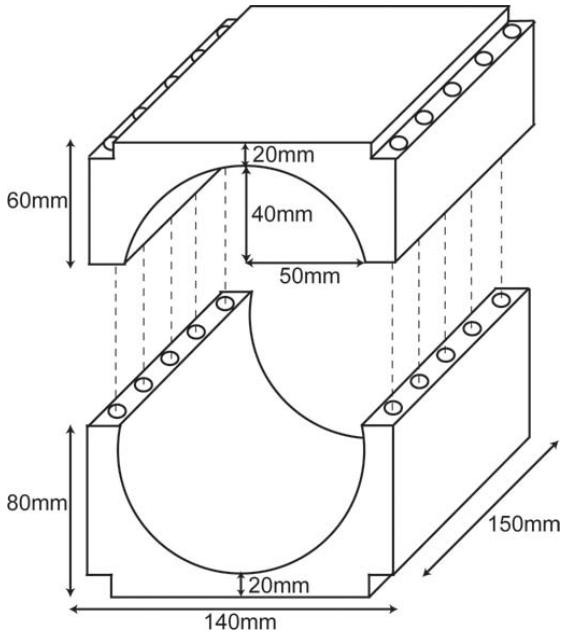

Figure 5. A diagram illustrating the main features of the sample holder.

2.5 Projectiles

The projectiles used in these experiments are mild steel projectiles with a diameter of 10 mm and a length of 100 mm. An aspect ratio of 10 makes the projectiles aerodynamically stable, both when flying through the air and when penetrating the sand samples. The diameter of 10 mm is one tenth of the diameter of the target, this allows significant penetration to occur before compaction waves reach the confinement of the sample holder. To lighten the projectiles, while maintaining their strength and stability, cylindrical cavities were bored into the rear section of the projectiles with diameter 4 mm and depth 63 mm. This gives an average projectile mass of 55 g and a centre of mass 3/8 of the way from the tip.

Two different types of projectile were used, flat ended and Ogive 2. The flat ended projectiles were simply sections of steel rod. The ogive projectiles had sharpened nose cones such that the nose profiles were surfaces of revolution of a circular arc. The radius of curvature of the circular arc was 20 mm, twice the diameter of the shaft of the projectile. The design of the ogive projectiles is shown schematically in figure 6.

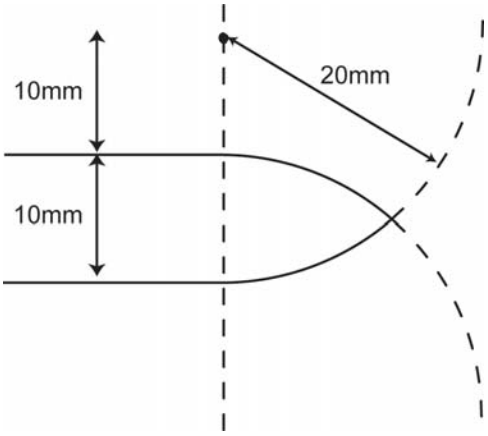

Figure 6. An ogive 2 rod tip

2.6 The Light Gas Gun

The projectiles were fired using the light gas gun facility at the Cavendish Laboratory. The light gas gun is a single stage gun with a six litre firing reservoir. The gun uses Helium gas and can be fired at pressures of up to 80 bar. A smooth bore barrel with a diameter of (10.5 ± 0.2) mm and a length of 2 m was used to accelerate the projectiles. The velocity of the projectile upon leaving the barrel of the gun is measured using two light gates consisting of laser diodes and detectors and separated by 10 mm. When connected to detector electronics these produce a top hat voltage with a duration equal to the time difference between the first and second light gate being broken. Preliminary experiments showed that a reliable velocity of (200 ± 5) m/s could be achieved using this setup.

2.7 Impact Chamber

The standard impact chamber used on the light gas gun is designed primarily for strength and its ability to hold a vacuum. Once an experiment has been set up it is very difficult to alter anything within the chamber. When carrying out DSR it is effectively impossible to remove the X-ray cassette from beneath the sample without disrupting the sample alignment and the fiducial markers. If the sample alignment is altered between the reference image and second image it is unlikely that the DICC algorithm will work effectively. Particularly, if a rotation of more than 5 degrees is introduced relative to the position in the reference image the errors in DICC become unacceptable.

A new impact chamber specifically designed for use in DSR was built. A side view of the new catch chamber, with the side removed, was shown in the previous progress report. The main improvement made is an enclosure within the chamber for holding the X-ray cassette, which can be accessed directly through the side of the chamber. This allows the X-ray cassettes to easily be switched after taking the reference image, without having to open the chamber. The sides of the chamber can be easily removed, allowing a plastic side to be used if high-speed photography or video of the impact is required. The new chamber is designed to accept a detachable alignment rig which allows for easy and accurate alignment of the sample.

2.8 Alignment Rig

For reproducibility between experiments it is necessary to precisely align the sample, so that the same location can be impacted in each experiment. To achieve this as accurately as possible, an alignment rig was designed to allow alignment of the sample to an accuracy of a few millimetres. The alignment rig, pictured in figure 7, consists of a turntable that can freely rotate 360~degrees, resting upon three screws. By adjusting the three screws, the sample can be made horizontal to within an accuracy of a few degrees.

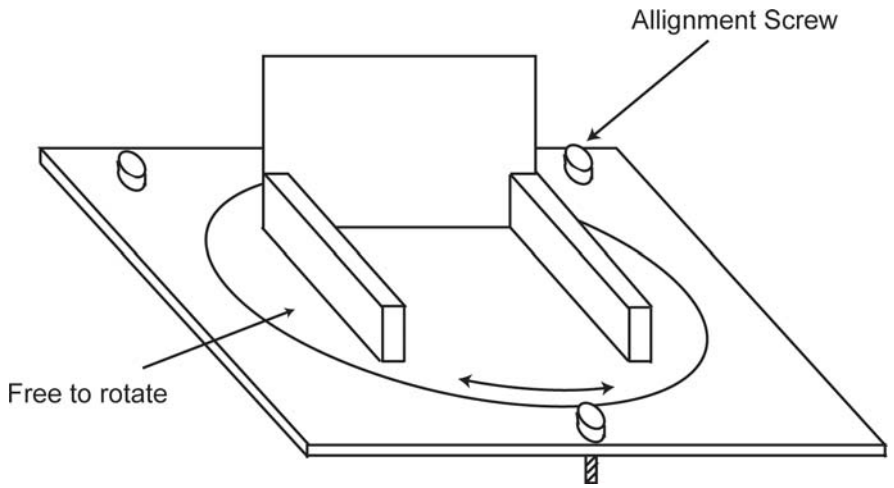

Figure 7. A diagram illustrating the main features of the sample alignment rig

A laser with a spot size of a few millimetres is shone down the central axis of the gas gun barrel onto the front of the sample. This allows the centre of the front face to be aligned with the central axis of the barrel. A mirror fitted to the front of the sample can be used to further align the sample such that the laser light is reflected back down the barrel. This ensures that the sample is flat and is aligned with its central axes parallel to, and overlapping, the central axis of the gun barrel. This confirms that the projectile will impact the centre of the front face and will travel along the central axis as desired. Two

photographs in figure 8 show the sample being aligned and the aligned sample with a make trigger fitted.

(a) (b)

Figure 8. Photographs showing the front of the sample during the alignment process. In (a) a laser beam is used to align the front of the sample, in (b) a make trigger has been added to the sample.

2.9 Sample Preparation

The two sections of the sample holder are temporarily sealed at the ends using thin pieces of card, allowing them to be filled with sand. As the sand is added they are tapped regularly on a hard surface, to cause the sand to settle. The larger section is initially filled with sand up to the original centre line of the cylindrical bore, 10 mm below the lip. A scattering of lead shot, with a coverage of 30% by volume, is randomly distributed over the surface to produce the speckle pattern. The section is then topped up with sand so that the surface is flush with the top of the section.

Once the smaller section is filled with sand, a Mylar sheet is secured over it to enclose the sand. It is then turned over and placed on top of the larger section to complete the cylinder. The Mylar sheet is removed, and the two sections of the sample holder are secured by tightening 10 bolts, 5 along each side of the holder. The temporary card is replaced with pieces of corrugated card, attached to the ends of the holder with epoxy. On the impact face a small section of the corrugated card is cut out and is replaced with thinner card, in order to avoid slowing down or disturbing the flight of the projectile at the moment of impact (this can be seen in figure 8 (b)).

2.10 Experimental Procedure

Once the sample has been prepared it is placed in the alignment rig, within the catch chamber, and is correctly aligned. A photograph showing the chamber set up ready for an experiment is given in figure 9.

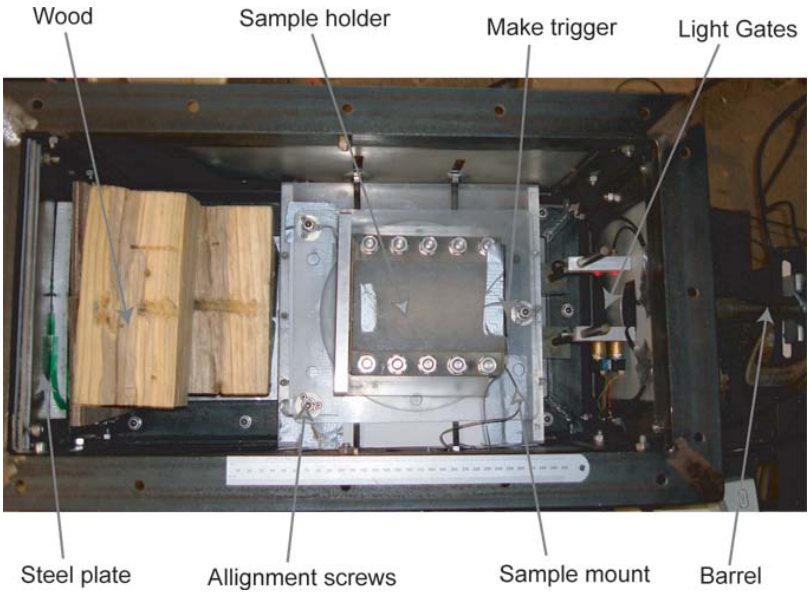

Figure 9. A photograph showing the inside of the catch chamber with everything set up.

A reference image for DSR is produced by taking an X-ray of the sample once the chamber has been closed and the lid fitted. A make trigger fitted to the front of the sample is used to trigger the X-ray system. The make trigger consists of two sets of interleaved copper threads such that there is no electrical contact across the trigger. When a metal projectile impacts the make trigger an electrical connection is made and this signal is used to trigger the X-ray system. A delay of any length can be added before firing the flash X-ray system, this allows X-rays to be taken at any time following the moment of impact.

3. Experimental Results

In order to build up a series of images showing the temporal progression of the penetration process a series of experiments need to be carried out with increasing X-ray delay times. Initially experiments were carried out using the flat ended projectiles. Delay times of 150 μs, 250 μs, 350 μs, 450 μs, 550 μs and 750 μs were chosen. By 750 μs the projectile is nearing the rear surface of the sample and the compaction waves have had sufficient time to interact with the boundaries.

As an example the reference X-ray and dynamic X-ray images, showing the penetration occurring at a delay of 350 μs, are shown in figure 10. The speckle pattern formed by the lead shot is clearly visible, as is the rod penetrator in the second image. The velocity of the projectile in this impact was (204 ± 2) m/s. In figure 11 is an X-ray from the side of the sample showing the layer of lead within this sample before the experiment. It can be seen from this X-ray that a relatively flat and thin layer of lead has been successfully achieved. The X-ray images are scanned into a computer using a transmissive scanner at a resolution of 300 dots per inch. DICC is carried out on the images in order to determine the internal displacements.

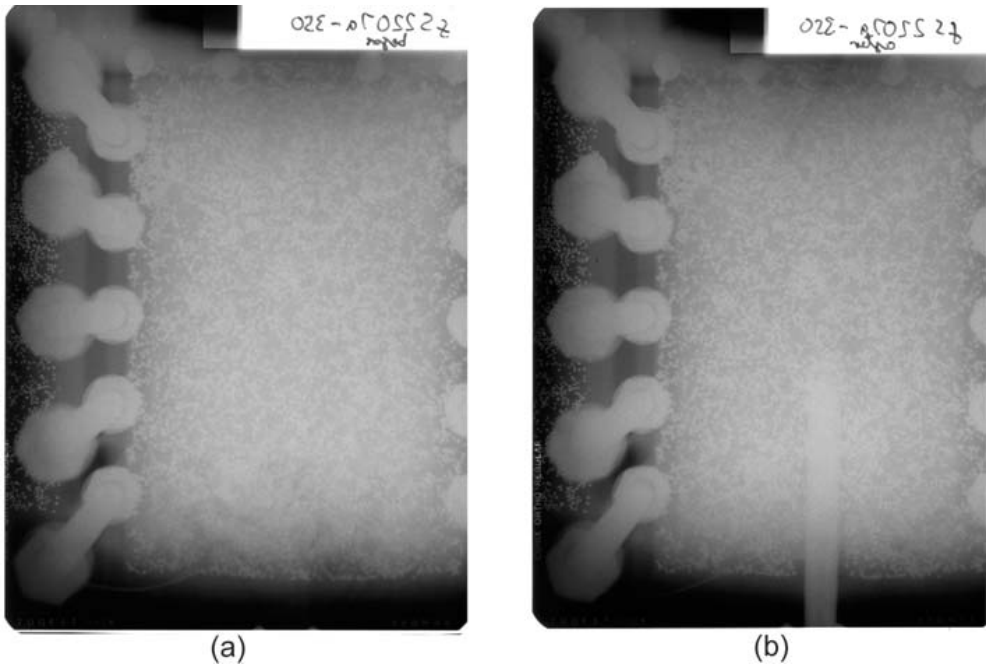

Figure 10. (a) The reference X-ray, (b) An X-ray taken at 350 μs after impact.

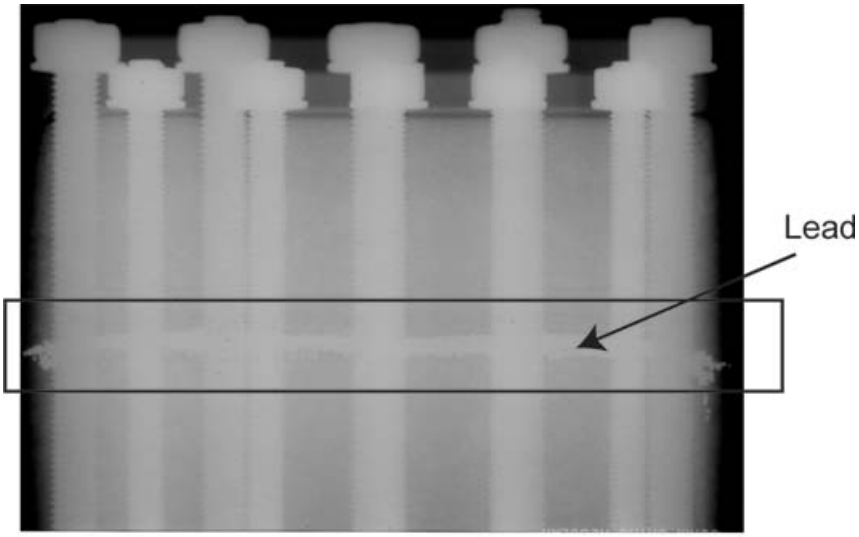

Figure 11. An X-ray of a sample from the side showing the layer of lead.

When analysing scanned X-ray images it often becomes obvious that there has been some small rotation of the images, either during the experiment or during the scanning process. Simple translations of the images can easily be accounted for, rotations can be more troublesome given that the position of the axis of rotation is unknown, as is the extent of the rotation. Small rotations can be corrected for using a plane fitting program. A section of speckle that is not deformed between images is required, this can either be a section near the back of the sample for small penetrations or a separate area outside the sample that has been seeded with lead to produce fiducial markers. The section is correlated and planes are fitted to the dx and dy displacements, any small rotation can be broken down into a combination of two such planes. The displacements due to rotation in the rest of the image can then be extrapolated. This method works well at correcting for small rotations, but errors of the order of a few pixels are introduced when dealing with larger rotations.

Once the data has been analysed the corrected displacements can be displayed as quiver plots. The total displacement at a given point in the material is shown as an arrow pointing in the direction of the displacement, with a length proportional to the magnitude of the displacement. Where the correlation has not worked correctly and given spurious displacements they have been set to zero. This occurs mainly in the area directly impacted by the projectile where the sub-images are deformed and sheared to such an extent that correlation is no longer possible. In figures 12 and 13 are scaled quiver plots showing the displacement maps for penetration by flat ended projectiles, with speed of (200 ± 4) m/s, at delays of 150 to 750 μs.

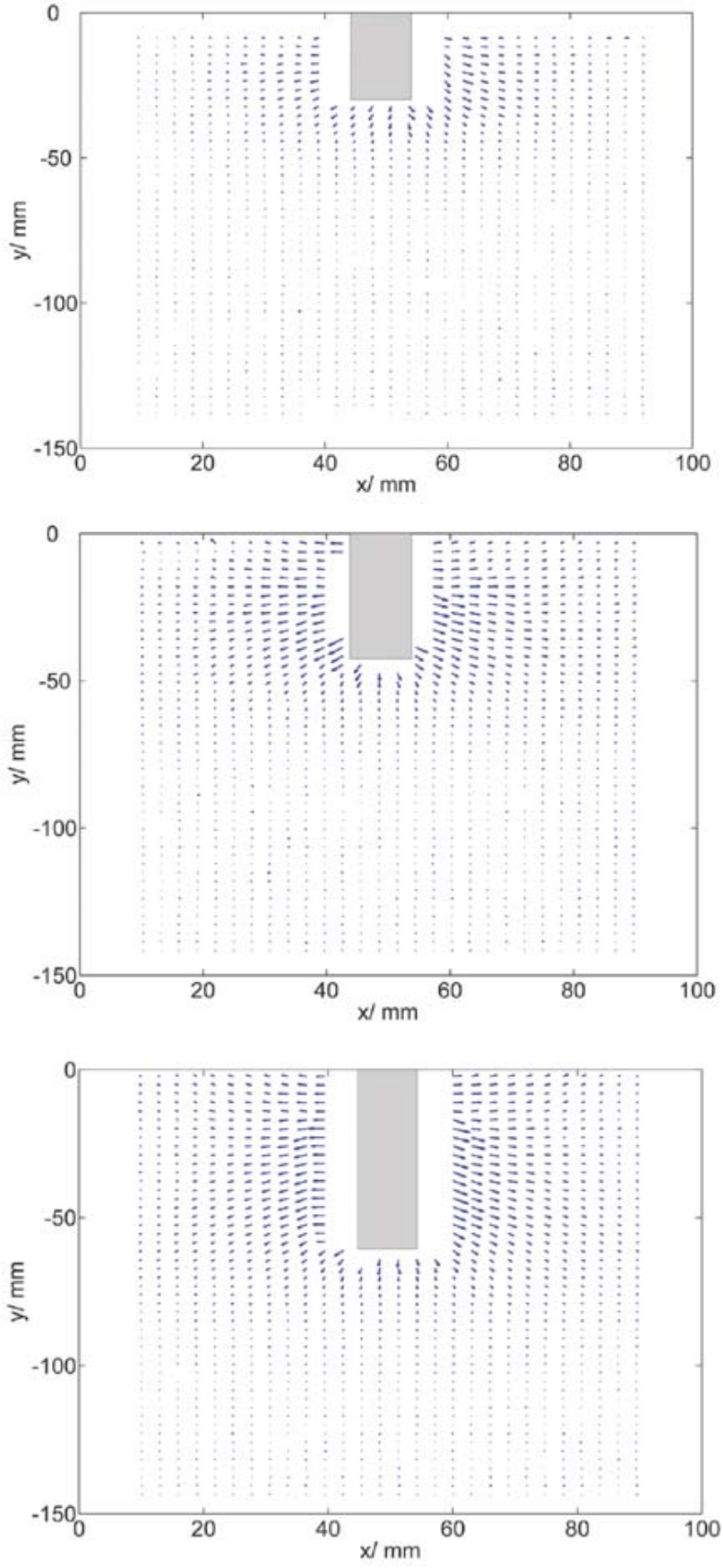

Figure 12. Scaled quiver plots showing penetration by a flat ended rod at 150, 250 and 350 μs after impact.

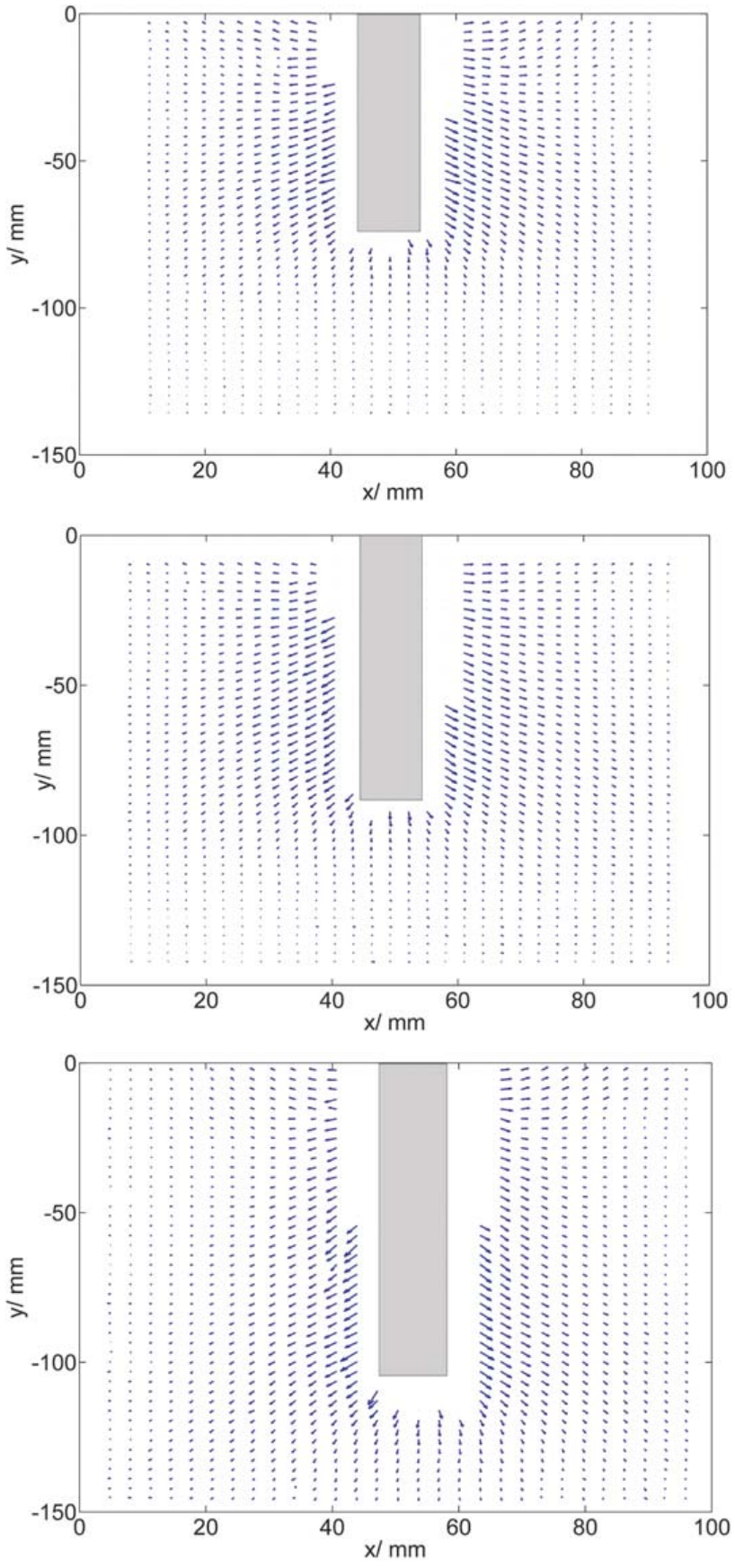

Figure 13. Scaled quiver plots showing penetration by a flat ended rod at 450, 550 and 750 μs after impact.

The initial response of the material is to flow away from the projectile. This includes material moving sideways away from the shaft of the projectile, forward ahead of the projectile, and even backwards for material at the impact surface. Let us consider first the displacements after 150 μs, shown in the first image of figure 12. The deformations are approximately symmetrical around the central axis of the rod, which is to be expected from conservation of momentum.

The lateral displacement of the sand closest to the shaft of the projectile ranges from 0.8 to 1.2 mm in magnitude. These displacements decay rapidly as the lateral distance from the rod increases so that at a distance of roughly 40 mm out sideways from the rod there is no lateral motion. Interestingly, there is also lateral displacement of the material directly ahead of the rod tip with magnitude of around 1 mm. The material directly ahead of the rod tip is being split laterally.

The largest longitudinal displacements are found directly in front of the rod tip. These range from 1.5 to 1.8 mm in magnitude. This is logical, as a flat ended rod is likely to push material ahead of it to some extent. The longitudinal displacement in front of the rod tip decays rapidly with increasing distance from the tip, only 25 mm in front the material appears largely undisturbed. There appears to be a curved front emanating from the point of impact with the front surface behind which material is moving longitudinally. This front appears to have reached a distance around 20 mm ahead of the rod tip at this stage (150μs after impact).

The same curved front of material moving longitudinally is seen in the second image in figure 12, showing the displacements after 250 μs. In order to more easily consider the longitudinal (dy) and lateral (dx) motions contour plots for the 250, 350 and 450 μs impacts showing the dy and dx displacements separately are shown in figures 14 and 15 respectively. Considering the first image in figure 14, showing the 250 μs case, the curved front envelope for material moving longitudinally can clearly be seen. The longitudinal displacements directly in front of the rod have increased to around 2.5 mm. The extent to which the deformation precedes the rod tip has also increased somewhat to around 30 mm. It is also apparent from this image that some of the material near to the impact surface is moving in the opposite longitudinal direction to the rod, by as much as 0.5 mm.

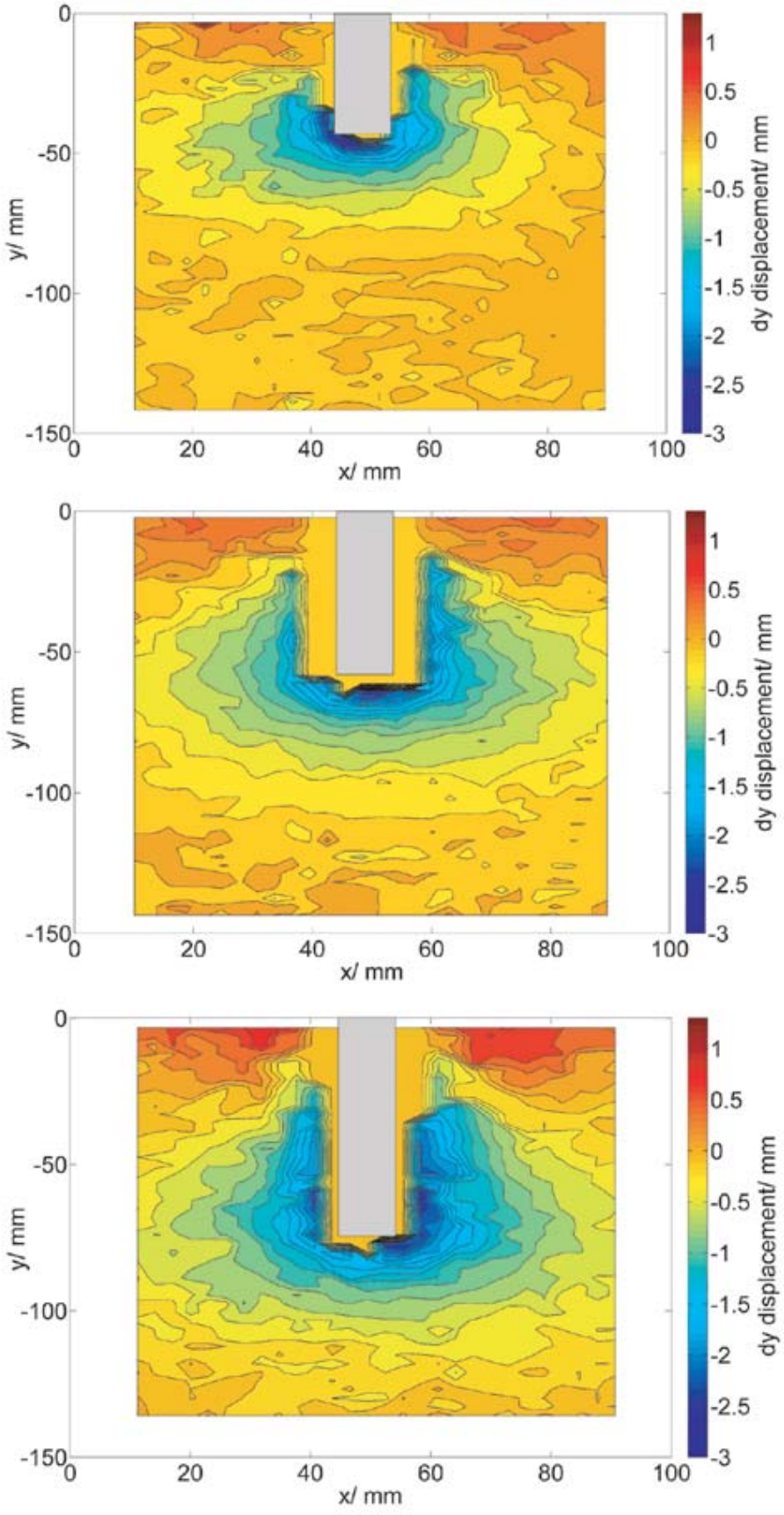

Figure 14. Contour plots of the dy (parallel to the rod) displacements for delays of 250, 350 and 450 μs.

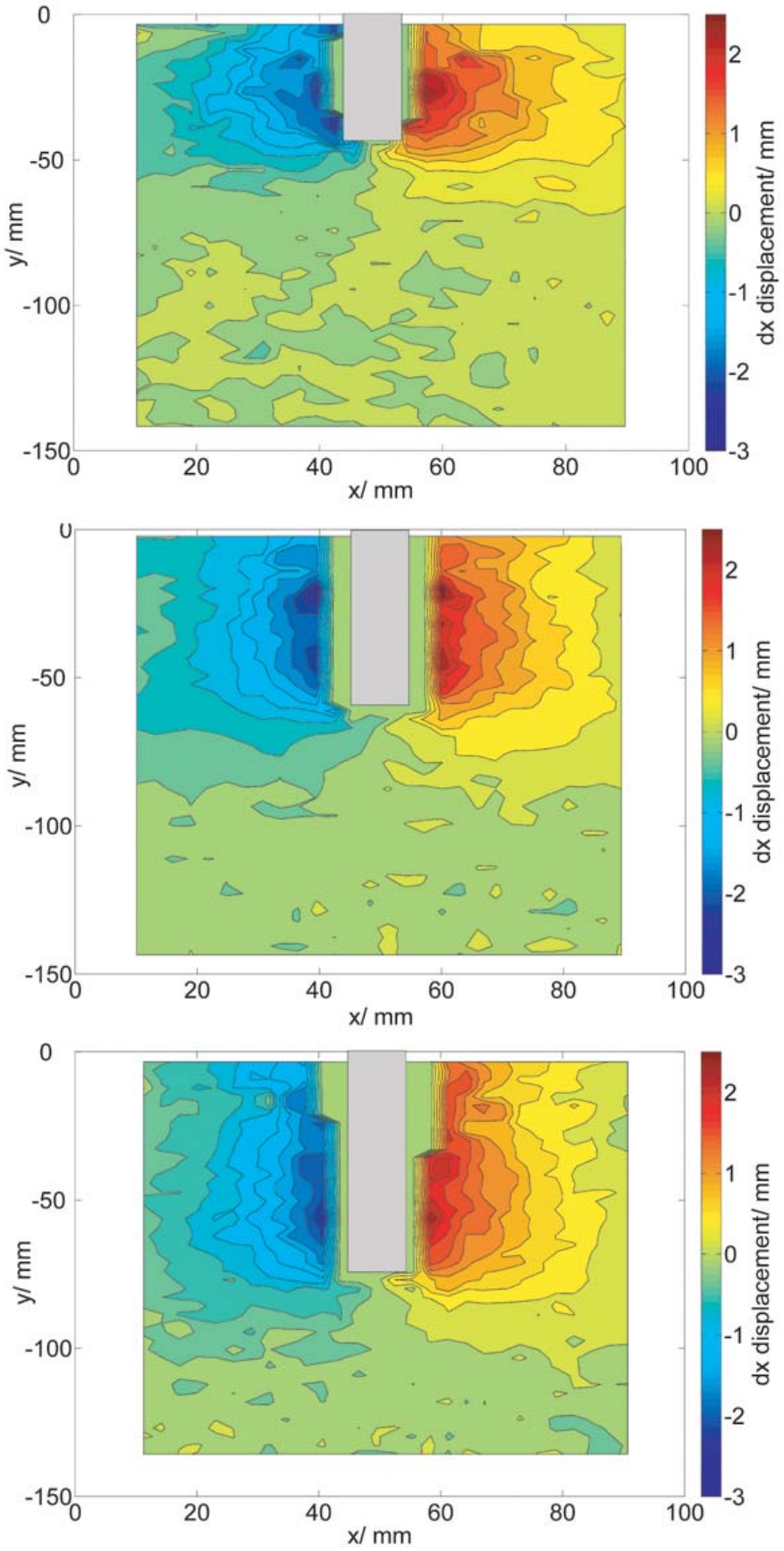

Figure 15. Contour plots of the dx (perpendicular to the rod) displacements for delays of 250, 350 and 450 μs.

The maximum transverse displacements at 250 μs are to the sides of the shaft where displacements of up to 2.4 mm occur. In the first image in figure 15 the symmetry of the transverse displacement becomes more apparent. The transverse displacements are relatively uniform along the length of the shaft, although they are reduced somewhat near the impact surface and near the tip of the rod. In all cases the transverse displacement is seen to extend somewhat ahead of the rod tip, apparently separating the material directly ahead of the rod.

As the penetration continues the images in figure 14 show the growth and development of the area of material moving in the longitudinal direction. The general shape of this area remains the same. There is a clear envelope consisting of a curved front which has emanated directly from the point of impact on the front surface. The edges of the curved front of the envelope are connected to this point by straight lines which make a roughly constant angle with the rod axis through the sequence of images. The angle made relative to the rod axis of the outer edge of the 0.2 mm displacement contour versus time delay is shown in table 2.

Delay/ μs	Angle/ degrees
150	39.8
250	43.1
350	39.8
450	39.8
550	37.1

Table 2. The angle of the envelope of dy displacements relative to the rod axis

The data show that the angle of the envelope remains relatively constant at (40 ± 2) degrees. This supports the suggestion that there is indeed a travelling front which has emanated from the point of impact, and which precedes the projectile tip, behind which material has moved longitudinally. An illustration showing how this envelope would look in three dimensions, assuming axial symmetry, is shown in figure 16. It can be seen from the contour plot in figure 17 that when considering the total magnitude of the displacement at a given point in the plane this travelling front is also clearly visible.

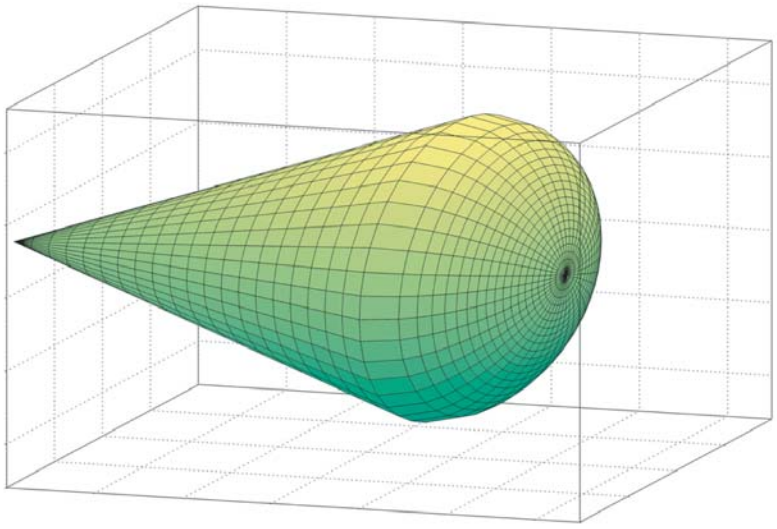

Figure 16. Illustration of the 3D envelope of material moving longitudinally

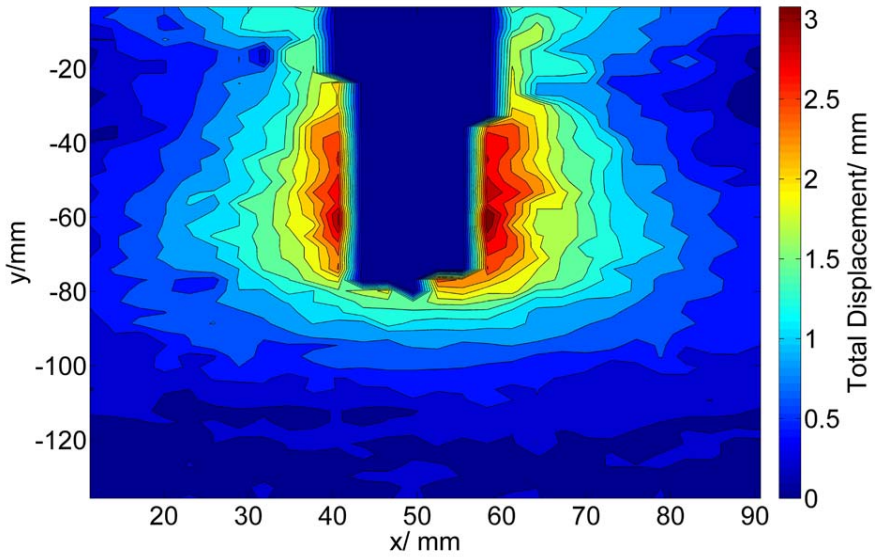

Figure 17. Contour plot of the total magnitude of displacement having occurred by 450 μs

After 150 μs the longitudinal motion extends to a distance of around 20 mm ahead of the rod tip. By 250 μs this distance has increased to around 30 mm, this distance then appears to remain constant throughout the rest of the penetration process (at least up to 550 μs). The maximum measurable displacement directly in front of the rod tip also remains fairly constant at around 2.5 - 3 mm. Some caution is required when interpreting this fact though. There is always an area directly in front of the rod where the sub-images do not correlate due to the excessive deformation. The maximum measured deformation here is therefore not necessarily the actual maximum displacement occurring. The area, first seen at 250 μs, of material moving in the opposite direction longitudinally to the rod appears to increase somewhat during the sequence of quiver plots. It can be seen that by 450 μs most of the

first 15 - 20 mm of the material is moving in the opposite direction to the rod by up to 1.5 mm.

Considering the three images in figure 15 it can be seen that the general shape and extent of the dx displacement envelope does not change dramatically during the sequence. The maximum transverse displacement remains fairly constant at around 2 mm from 250 μs onwards. The extent to which the envelope of transverse displacements extends to the sides of the remains relatively constant also at around 40 mm. It can be seen that the symmetry of the displacements appears to be roughly maintained throughout all of the quiver plots.

For some of the experiments carried out high speed video was taken using a Photosonics Phantom V4.3 high speed video camera. In figure 18 are three images from a larger sequence showing the penetration of a sample by a flat ended projectile. These images were taken at 16,000 frames per second giving an inter-frame time of 63 μs. What is clear from these images is that while the projectile is entirely within the sample there is no outward sign that the penetration is occurring. This suggests that the amount of deformation occurring ahead of the projectile is limited (remember that the far side is constrained by card so the deformation may have reached the far surface and it just not visible). It is also clear that when exiting the rear surface of the sample the projectile takes a cone of material with it.

This can be seen in more detail in the images in figure 19 where the high-speed camera has been focused on the rear surface of the sample. When the projectile penetrates the rear surface of card, and exits the sample, it draws out sand with it so that a roughly cone shaped area of sand is moving with the rod.

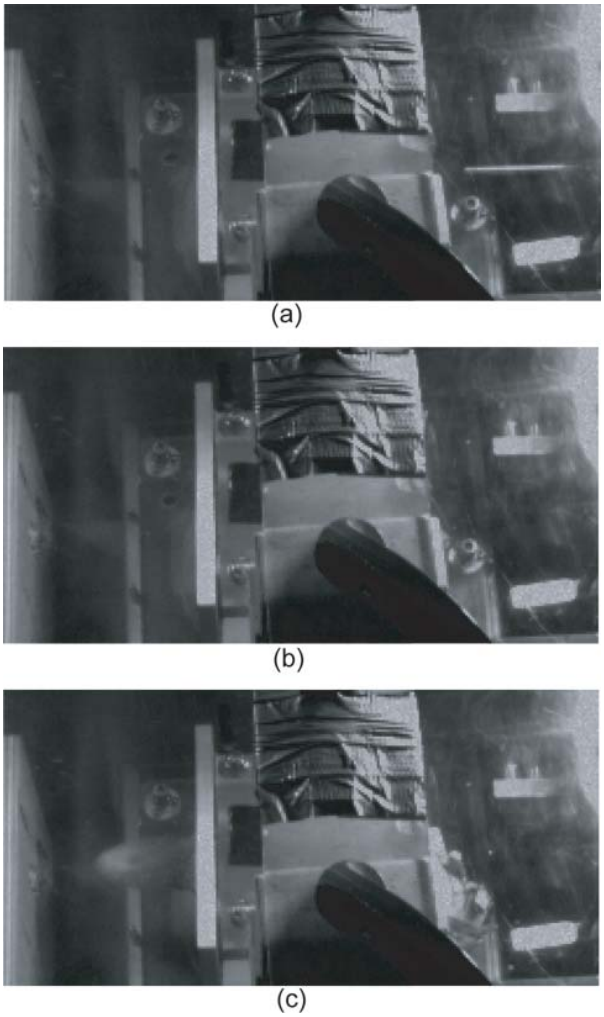

Figure 18. A sequence of high-speed video images showing penetration of the sample by a flat ended rod. The images show: (a) The moment before impact. (b) The rod entirely within the sample. (c) The rod exiting the sample.

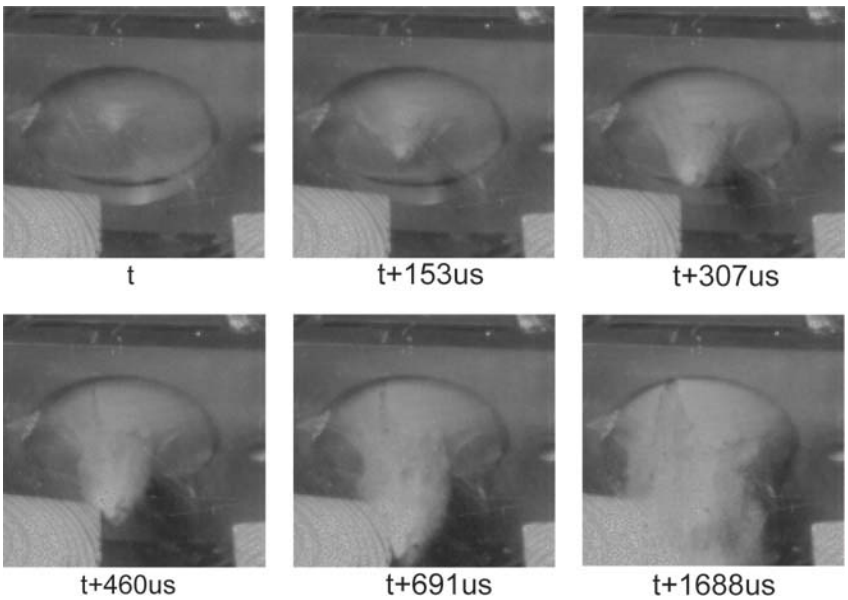

Figure 19. A sequence of high-speed video images showing a flat ended rod exiting the back of the sample.

The depth of penetration at a given time can be measured from the X-ray images. Care must be taken with some images as there appears to be a cone of denser material at the rod tip which can increase the difficulty of identifying the location of the rod tip. A graph showing the penetration depth of the flat ended rod versus the time since impact is shown in figure 20. This graph shows a change in gradient at 150 μs and an apparently constant gradient for the remainder of the graph. Using the measurements of penetration depth versus time it is possible to estimate the instantaneous velocity of the projectile for a series of penetration depths. This is plotted in the graph shown in figure 21.

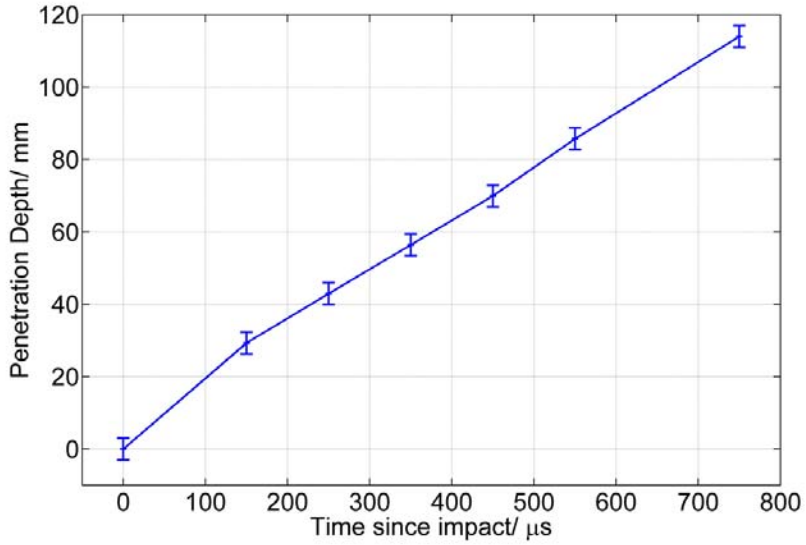

Figure 20. A plot of penetration depth versus time since impact for the flat ended rod.

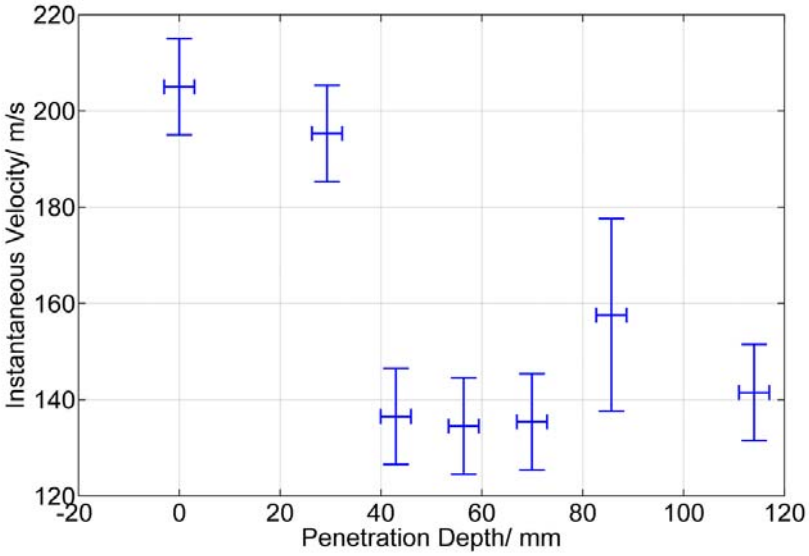

Figure 21. A plot of instantaneous velocity versus penetration depth for the flat ended rod.

The velocity data shows that there is a considerable decrease in the velocity of the penetrator between a depth of 20 - 40mm (corresponding to between 150 and 250 μs after impact). The velocity falls from around 200 m/s to around 140 m/s. What is then somewhat surprising is that the velocity of the projectile appears to change little after this initial decrease, remaining fairly constant around 140 m/s up to 750 μs (the velocity at 550 μs appears anomalous, it is particularly difficult to locate the tip of the rod in this image). This suggests that the rod feels a considerable force during the early stages of the penetration, but that after 250 μs the rod experiences little further force. Therefore the rod and the surrounding sand have reached an equilibrium, such that little further energy is exchanged between them.

The distance in front of the rod at which material is at rest seems to remain fairly constant from 250 μs onwards. In order to investigate this further it is informative to look at the displacements in the longitudinal direction, along a line running directly from the rod tip to the rear surface of the sample. This is plotted for five different time delays in figure 22. The amount of material being moved longitudinally in front of the rod increases between 150 and 250 μs, but then remains relatively constant for the remainder of the penetration process. After the initial stages of the impact a steady state is reached where a constant amount of sand is being pushed in front of the rod. This agrees well with the velocity data obtained earlier. Both data sets suggest an equilibrium situation is reached around 250 μs, and that the penetration continues approximately in a steady state between 250 and 750 μs.

As an aside, it is interesting to note that the profiles shown in figure 22 are well fitted by exponential curves. The exponential plots fitted to the last four curves in figure 22 all have very similar exponential factors of (-0.068 ± 0.003) , the first has a noticeably more negative exponential factor of -0.112. Once again this suggests that the way in which material is being affected ahead of the projectile changes between 150 and 250 μs, but then remains relatively constant. Exactly why the displacements decay in an exponential manner like this is not immediately clear.

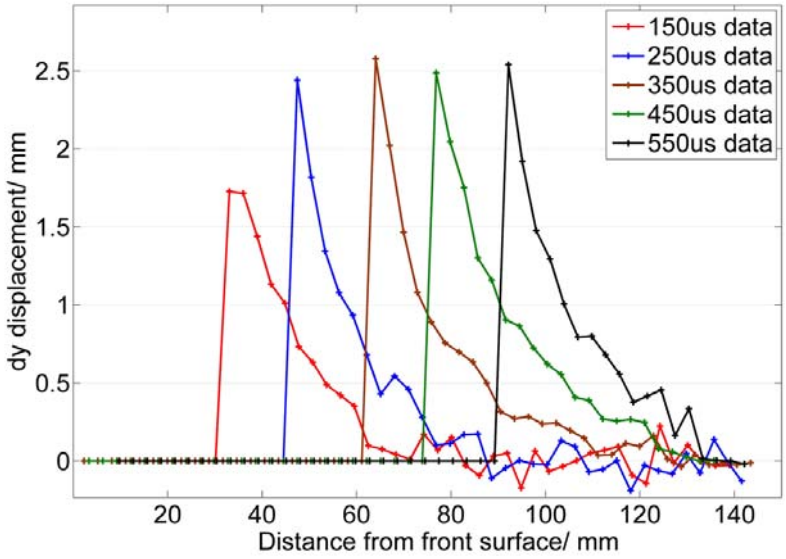

Figure 22. Plots showing how the longitudinal displacement (parallel to the rod) varies with distance in front of the rod tip.

4. Preliminary Conclusions

Before moving on to consider the effect of projectile nose shape on the penetration properties it is worth summarising what we have learned so far. It has been seen that applying DSR to study the penetration of granular materials has provided high resolution data showing the displacement fields within a plane. This data provides considerable information regarding the response of the material to penetration and allows us to see exactly how the material is deforming.

Considering the lateral displacements first, we have seen that the lateral displacements appear to vary uniformly with distance out from the rod for almost the entire length of the rod. This suggests that the lateral displacement is being caused by the movement of the tip of the rod, once this has passed little further lateral displacement is occurring. We have seen that in all of the images there is lateral displacement occurring directly in front of the rod tip, this splits the material ahead of the rod and reduces the amount of material that is pushed ahead of the rod. There is a gradient in the lateral displacements suggesting that compaction of the material is occurring. This is unsurprising, as a loosely packed granular material such as this will contain a number of voids between sand grains. When the sand grains are given energy they are able to re-arrange themselves into a more closely packed arrangement and therefore reduce the sizes of these voids.

When considering the longitudinal displacements, and indeed the total magnitude of the displacements, there is a clearly expanding envelope behind which material is in motion. This emanates from the point of impact and consists of an expanding cone with a curved front surface. The amount of sand which is moving increases between 150 and 250 μs but then remains relatively constant. The evidence suggests that during the early stages of the penetration, and the initial impact of the projectile with the front surface, a large quantity of sand is set in motion. This process generates significant resistive force on the projectile and causes it's velocity to fall sharply. The body of moving sand extends ahead of the projectile by up to 40 mm, this means that after the early stages of penetration the projectile is moving through sand that is also moving. This leads to significantly reduced resistive forces relative to the early stages, for a period of time the projectile has entered a form of steady state motion where little further energy is exchanged between the projectile and the surrounding sand. It is possible that the rigid cylindrical confinement is supporting this process, in a larger sample energy would likely be dissipated more in the surrounding material.

Clearly if the penetration was able to continue further dissipative processes such as compaction and shearing of the sand would slow the moving area of sand and the projectile would experience further resistive force. This does not appear to have occurred to a significant extent by 550 μs.

5. Effect of Nose Shape

An equivalent set of experiments to the ones discussed in the previous section were carried out using a projectile with an ogive 2 nose shape (100 mm length to the tip, 10 mm diameter). The series of quiver plots are shown in figures 23 and 24. A series of experiments were also carried out using projectiles with hemispherical nose cones, their deformation fields were not significantly different to the ogive ones so it was deemed unnecessary to carry out a full series of experiments. Instead high-speed video was used to monitor the penetration of the front surface in order to determine the velocity of the projectile during the penetration process. This allows for comparison with the velocity profiles for flat ended and ogive nose shapes but also provides an entirely separate method for measuring the velocity of a rod during penetration, therefore ensuring that the profiles derived from the X-ray data are correct.

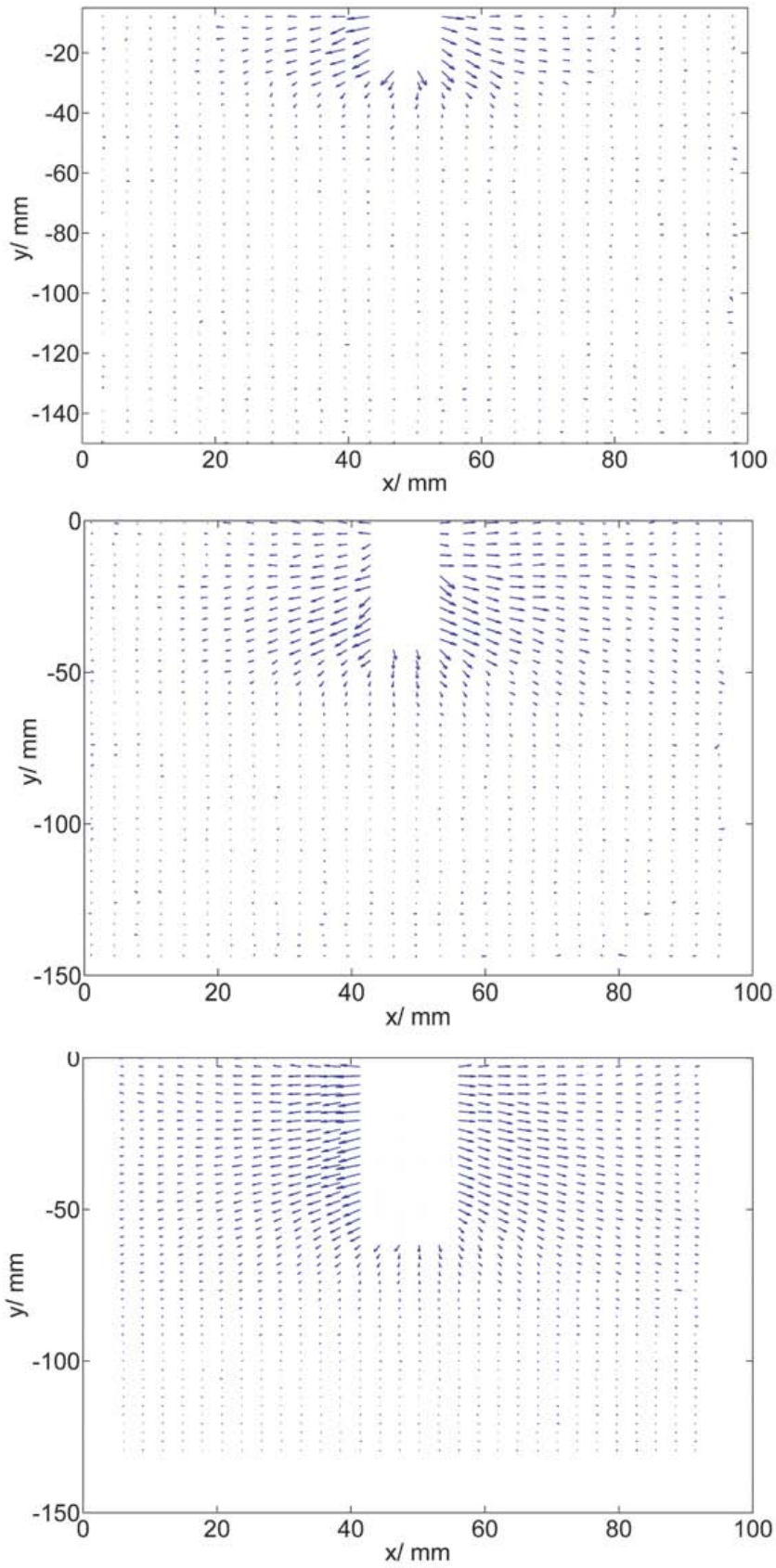

Figure 23. Quiver plots showing penetration by an ogive tipped rod at 150, 250 and 350 μs.

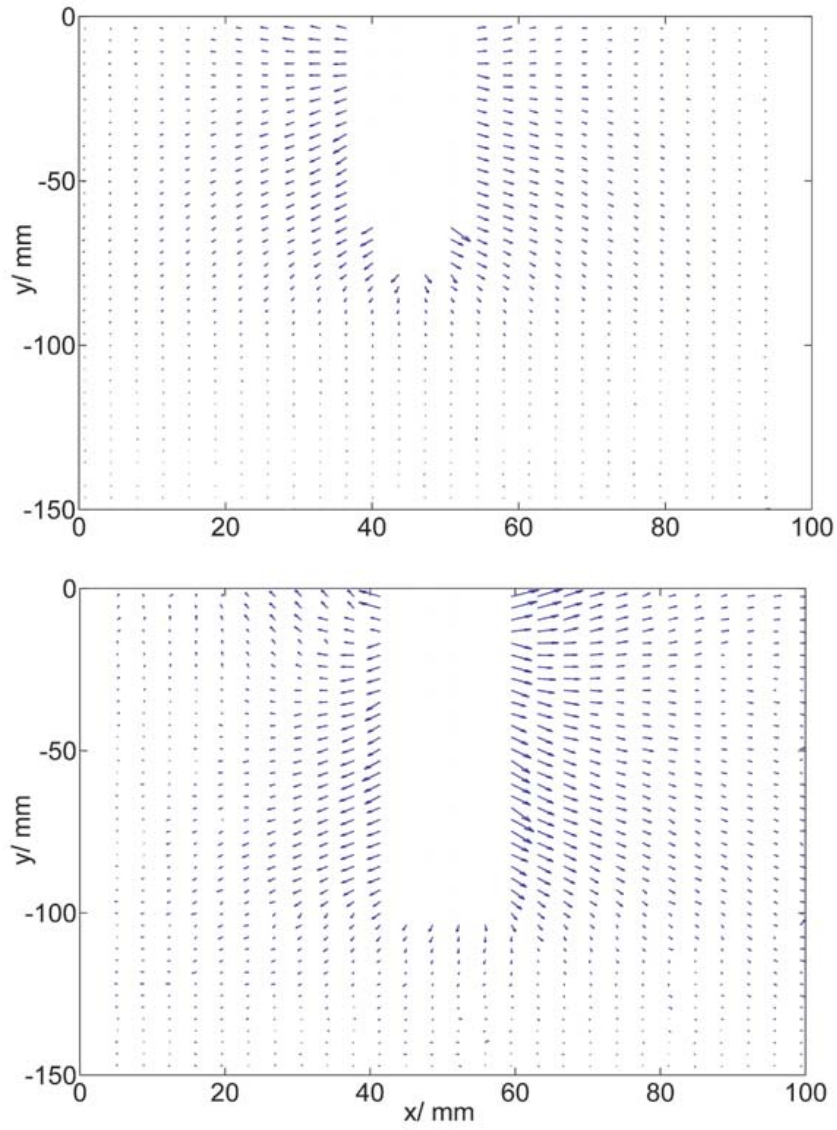

Figure 24. Quiver plots showing penetration by an ogive tipped rod at 450 and 550 μs.

Plots of the velocity versus penetration depth for the three different nose shapes are given in figure 25. The data for the flat ended and ogive rods was obtained from the X-ray images, the data for the hemispherical nose shape was obtained by measuring the position of the rod during the penetration on high speed video images. What can immediately be seen is that with all three of the nose shapes there is an initial considerable drop in velocity between 0 and 30 mm penetration depth, subsequently there is much less variation in the velocity. Interestingly though the final velocity at which the graphs seem to plateau is not the same for all nose shapes. For rods with flat ends a roughly steady state velocity of around 137 m/s is reached. for ogive and hemispherical rods a considerably higher final velocity of around 164 m/s is reached. Assuming the graphs are entirely flat for the final 4 - 5 data points (an unlikely assumption, but useful for comparative purposes) the final velocities are given in table 3.

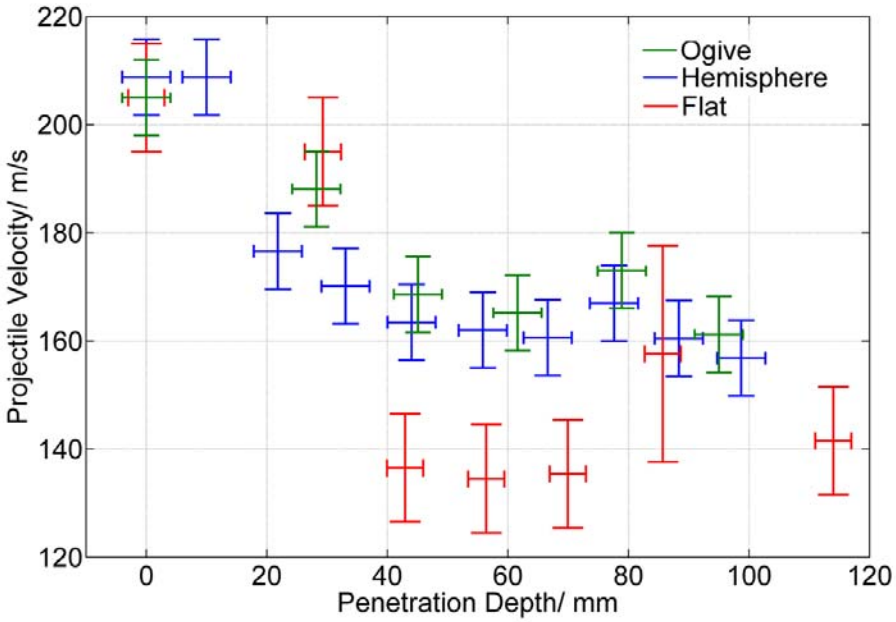

Figure 25. Velocity versus penetration depth for the three different nose shapes

Tip Shape	Final Velocity / m/s
Ogive 2	167 ± 5
Hemispherical	164 ± 8
Flat	137 ± 4

Table 3. Final 'steady-state' velocities

The final velocities measured for the rod with an ogive tip are generally higher than those measured for the rod with a hemispherical tip, although the errors are relatively large. What is clear though is that the final velocities for the flat ended rod are significantly lower. If the large initial drops in velocity are caused by the rods setting a large section of the sand into motion, this suggests that the ogive and hemispherical rods are setting a smaller mass of sand into motion than the flat ended rod. In order to investigate whether this is indeed the case for the ogive rod it is informative to consider some of the quiver plots in more detail.

Considering the first quiver plot in figure 23, showing the displacements after 150 μs, it can be seen that the pattern of displacements is similar to that observed for flat ended rods. The maximum lateral displacements close to the shaft of the rod range from 0.6 to 1.2 mm, again very similar. The maximum longitudinal displacements are found directly ahead of the rod tip and are around 1.8 mm. Comparing the quiver plot with the equivalent for the flat ended rod, shown in figure 12, it can be seen that the area in which the correlation fails is considerably narrower for the ogive rod. This suggests that

the extent of the deformation occurring in the area immediately around the rod is somewhat less in this case.

Moving on to consider the case at 350 μs, some further differences between the response of the sand to the two rod types become apparent. In figure 26 are shown the longitudinal (dy) and transverse (dx) displacements for penetration by flat ended and ogive tipped rods at 350 μs after impact. Firstly it is clear that the form of deformation occurring is similar for both rod types, the general shapes of the displacement fields are the same. From the dy displacement plots it can be seen that the deformation extends further ahead of the rod tip in the flat ended case. The deformation extends to a distance of around 40 mm ahead of the rod tip, for the ogive tip the deformation only extends to a distance of around 30 mm. This suggests that the flat ended rods are causing more deformation to occur in front of the projectile.

In order to investigate this in a little more detail it is helpful to look at the lateral (dx) and longitudinal (dy) displacements along a line ahead of the rod and perpendicular to the direction of motion of the rod (a line that is horizontal in the surface plots shown in figure15). This is done for a line 15 mm ahead of the absolute tip of the projectile for both the flat ended and ogive rod shapes, at a time of 450 μs, in the first part of figure 27. What is clear from this figure is that both the dx and dy displacements are larger ahead of the rod for the flat ended case, by almost a factor of two for the dy displacements.

This confirms that a flat ended rod does indeed disturb the material ahead of the rod to a greater extent. This increased disturbance is not found just directly ahead of the rod but across the whole width of the sample in front of the rod tip. For comparison in the second part of figure 27 are shown similar plots for a line 10 mm behind the rod tip. It can be seen from these plots that the dx and dy displacements are much more similar than those found ahead of the rod tip. This suggests that the displacements behind the rod tip are similar for both types of rod. The main differences in the behaviour of the two types appears to be explained by the amount of deformation being caused ahead of the projectile.

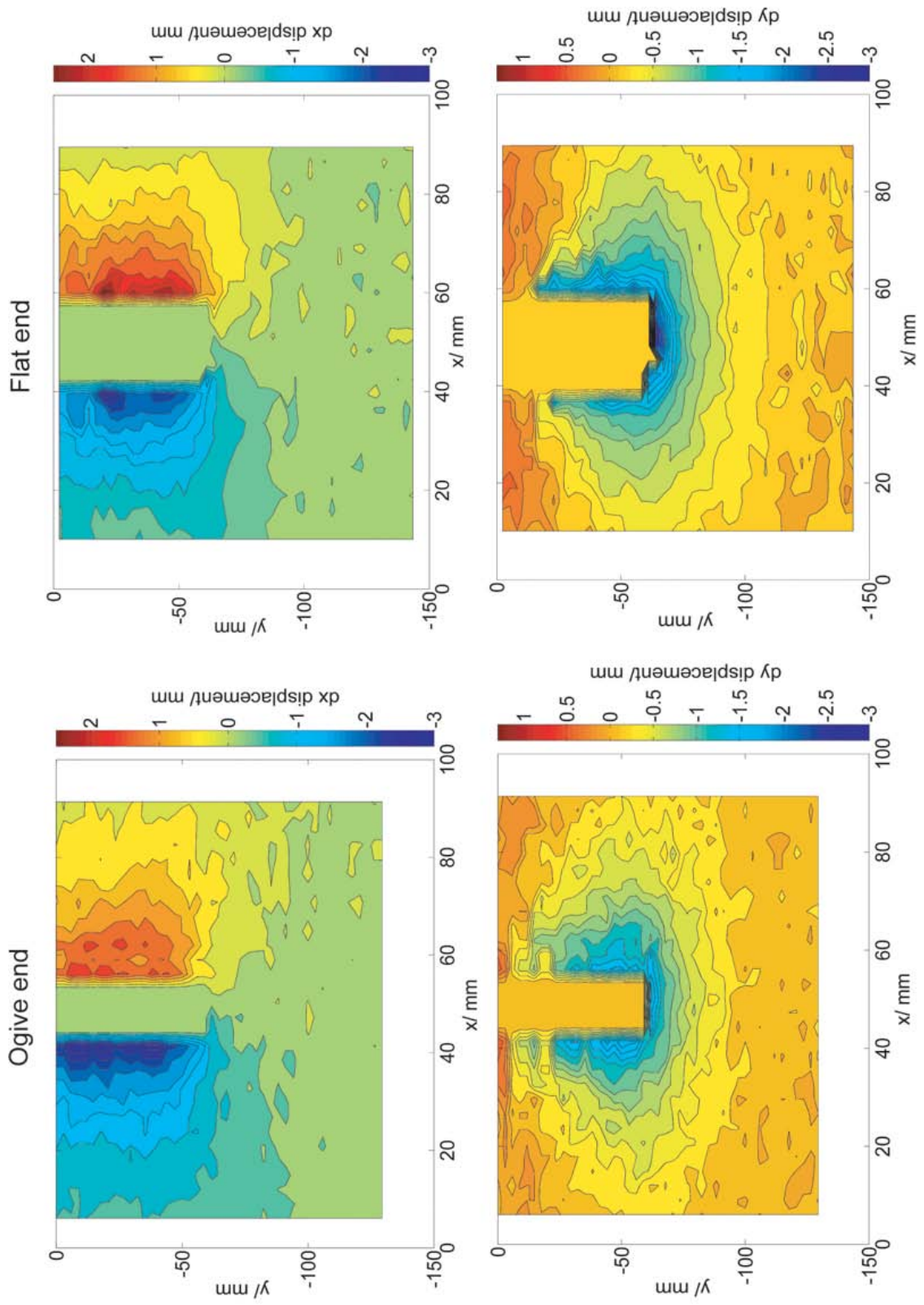

Figure 26. Comparing the displacements at a delay of 350 μs for flat ended and ogive end rods.

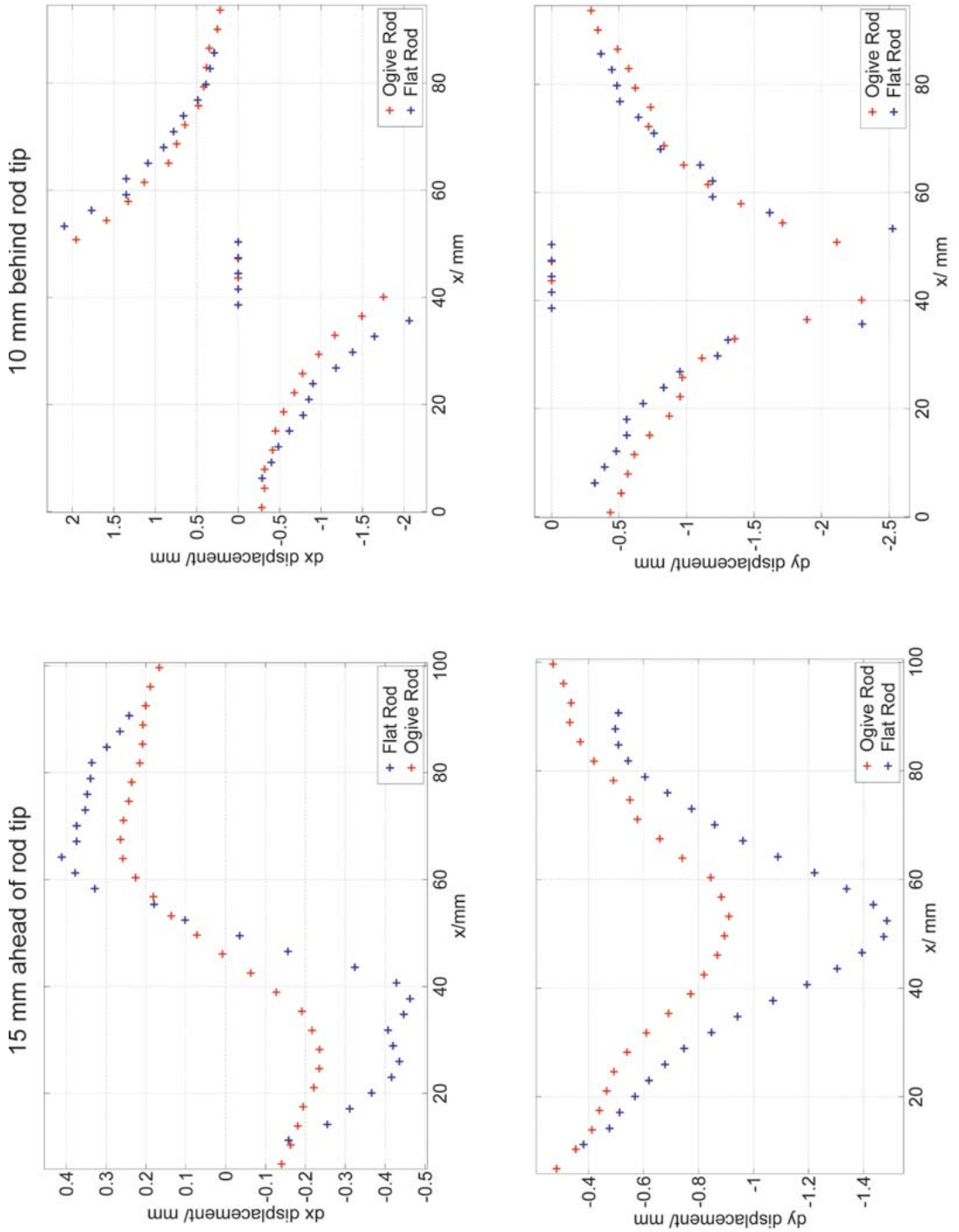

Figure 27. Comparing the dx and dy displacements along lateral lines ahead of and behind the projectile tips.

In the same way as with the flat ended rods (see table 2) it is useful to consider the angle the cone of longitudinal displacements makes with the rod axis at the various times, this is done in table 4.

Delay/ μs	Angle/ degrees
150	41.3
250	42.1
350	39.0
450	40.5
550	42.0

Table 4. The angle of the envelope of longitudinal displacements relative to the rod axis

The angle once again seems to remain constant at (41 ± 2) degrees, in good agreement with the value obtained for the flat ended rods ((40 ± 2) degrees). This would seem to suggest that the angle that this cone makes with the rod axis is some property of the sand and the size of the projectile, it is independent of the nose shape. The nose shape appears to affect how far ahead of the projectile tip these deformations extend.

6. Conclusions

We saw with a flat ended projectile that during the early stages of impact a large body of sand appeared to be set in motion, slowing the projectile significantly. Subsequent to this the projectile entered a steady state for a period of time where little further energy appeared to be transferred between the projectile and the surrounding material. This conclusion is strengthened by the subsequent data obtained showing the velocity versus depth profiles for a hemispherical ended and ogive 2 ended rod (figure 25). In both of these cases the same significant drop in velocity during the early stages, followed by a relatively constant velocity up 750 μs, was observed. It was observed that the initial drop in velocity was considerably larger for the flat ended projectile than for the other two types. This suggested that the flat ended projectile was setting a larger body of sand in motion during the early stages.

Considering the moment of impact, and the early stages of penetration, it can be seen that penetration by a flat ended projectile would be more like a plate impact, generating a large initial resistive force. A sharpened nose cone, as with the ogive tip, would lessen this initial moment of impact and therefore lead to a smaller initial resistive force. This is a similar effect to that well known to divers, the force on impacting the surface of the water is much reduced by adopting a streamlined shape relative to landing flat on your front or back.

Looking at the displacements ahead of and behind the projectiles seems to confirm that the main difference between the response of the sand to penetration by the two types of rod is the extent of deformation that is occurring ahead of the rod tip. The dx and dy deformations along a lateral line 10 mm behind the rod tips are very similar, coupled with the similar angle of the cone of displacement this suggests that the deformation behind the rod tip is very similar in both cases. The deformation occurring ahead of the rod tips though is significantly different between the two cases. For a flat ended rod the displacements extend at least an extra 10mm ahead of the rod tip relative to the ogive rod. Looking at the displacements along a line 15 mm ahead of the rod tips we have seen that significantly greater deformation is occurring ahead of the flat ended rod, particularly when considering the longitudinal displacements.

It appears that during the early stages of the penetration the flat ended rod impacts the surface and causes a large amount of sand to be set in motion, its flat surface means a considerable amount of longitudinal displacement directly in front of the rod occurs. This material moving forwards ahead of the rod pushes material laterally away from the rod ahead of the tip. When the ogive rod impacts the surface its streamlined nose cone means that is sets a smaller body of sand into motion, its curved surface means less material is pushed longitudinally ahead of the rod. This means that both the longitudinal, and therefore the lateral displacements, ahead of the rod are reduced relative to the flat ended case. As the ogive rod disturbs the material to a lesser extent it feels less of a resistive force and therefore maintains a higher velocity than the flat ended rod. In both cases once an initial body of sand has been set moving the rods are then travelling in moving material and therefore experience considerably reduced resistive forces. This means that in both cases a steady state is reached for a period of time where little further energy is exchanged between the rod and the surrounding material.